Fragment distribution in ^{78,86}Kr+^{181}Ta reactions*

Dong-Hong Zhang(张冬红)[1;1]   Feng-Shou Zhang(张丰收)[2,3,4]

[1] College of Physics and Electronics, Institute of Theoretical Physics, Shanxi Datong University, Datong 037009, China
[2] The Key Laboratory of Beam Technology and Material Modification of Ministry of Education,College of Nuclear Science and Technology, Beijing Normal University, Beijing 100875, China
[3] Beijing Radiation Center, Beijing 100875, China
[4] Center of Theoretical Nuclear Physics, National Laboratory of Heavy Ion Accelerator of Lanzhou, Lanzhou 730000, China

Abstract: Within the framework of the isospin-dependent quantum molecular dynamics model, along with the GEMINI model, the ^{86}Kr+^{181}Ta reaction at 80, 120 and 160 MeV/nucleon and the ^{78}Kr+^{181}Ta reaction at 160 MeV/nucleon are studied, and the production cross sections of the generated fragments are calculated. More intermediate and large mass fragments can be produced in the reactions with a large range of impact parameter. The production cross sections of nuclei such as the isotopes of Si and P generally decrease with increasing incident energy. Isotopes near the neutron drip line are produced more in the neutron-rich system ^{86}Kr+^{181}Ta.

Keywords: fragment distribution, heavy ion, quantum molecular dynamics

PACS: 25.70.Mn, 25.70.Pq, 24.10.-i   **DOI:** 10.1088/1674-1137/42/5/054107

1   Introduction

Research into new nuclides is an important subject in the field of nuclear physics [1]. With the emergence of more powerful detectors, the general characteristics of multifragmentation have been studied [2–6]. Further development in the future will be related to the study of many observations and the correlation of multifragmentation events. As an effective way to produce rare isotopes, nuclear multifragmentation plays an important role in the study of nuclear physics [7].

The stable nuclides are located in a narrow region of the nuclide map, and the line that runs through the center of the region is called the β stability line. The theoretical models of structures, such as the shell model, the liquid drop model, and the collective model [8], are based on the study of the nuclei located in the stability line and nearby. With the development of nuclear physics and the progress of accelerator and nuclear detection technology, many new nuclides have been synthesized by nuclear reactions [9, 10]. The nuclei on the nuclide map have been expanded in the direction of both proton number and neutron number.

In recent years, more and more attention has been paid to experimental and theoretical research on the exotic nuclei far away from the β stability line [11, 12]. The area of the nuclide map near the drip line has been of particular interest [13, 14], as it is very important for ex-

plaining the change of nuclear structure with the increase of neutron-proton ratio and the study of the mechanism of nucleosynthesis [15–18]. Therefore, it is of great significance to study the production of isotopes near the drip line.

This article is based on the isospin-dependent quantum molecular dynamics (IQMD) model along with the statistical decay model GEMINI to study the production cross sections of nuclides in heavy ion collisions. By investigating the reactions of different collision systems, the multiplicity, charge distribution and production cross sections of the nuclide near the drip line are calculated, and the production cross sections of the isotopes of Si and P are obtained. The results show that the production cross sections of isotopes in the reaction are related to the incident energy and the isospin of the collision system. The production cross sections of the isotopes of Si and P decrease with increasing energy, and the isotopes near the neutron drip line are more productive in the ^{86}Kr+^{181}Ta reaction than in the ^{78}Kr+^{181}Ta reaction.

2   Theoretical framework

Since the fragments are produced in kinetic reactions, it is necessary to develop micro-kinetic models to study the formation of fragments [19–21]. Some of the existing models are based on statistical descriptions of multi-body phase space calculations [22–26] and oth-

ers are molecular dynamics models [27–29] or stochastic mean field models [30, 31] that describe the dynamical evolution of the system in nuclear collisions. The first method uses the equilibrium state statistical mechanics method to study the thermodynamic description of finite nuclear systems. The second method is a complete description of the temporal evolution of the collision system and is therefore useful for studying nuclear species, finite-size effects, kinetics of phase transitions and so on. The empirical parameterization of fragment cross sections can help to predict the mass and charge distribution of heavy ion reactions. Statistical models can reproduce the experimental results of heavy ion collisions. Molecular dynamics models include information about the transport mechanism. Examples are the micro-antisymmetric molecular dynamics model [32] and the fermionic molecular dynamics model [33]. The isospin-dependent Boltzmann-Langevin equation (IBLE) model [34] can also be used to calculate the cross section of fragments. The quantum molecular dynamics (QMD) model and statistical decay model GEMINI are used to describe heavy ion reactions.

The IQMD model [35] considers isospin freedom on the basis of QMD, which contains the isospin degree of freedom of the nucleons. The IQMD model can be applied to the study of many heavy ion collisions at intermediate energy. A multi-body theory for simulating heavy ion reactions with incident energies between 30 MeV/nucleon and 1 GeV/nucleon, the IQMD model uses Gauss wave packets to describe every nucleon

$$\phi_i(\boldsymbol{r},t)=\frac{1}{(2\pi L)^{3/4}}\mathrm{e}^{-\frac{[\boldsymbol{r}-\boldsymbol{r}_i(t)]^2}{4L}}\mathrm{e}^{\mathrm{i}\frac{\boldsymbol{r}\cdot\boldsymbol{p}_i(t)}{\hbar}}, \qquad (1)$$

where $\boldsymbol{r}_i$ and $\boldsymbol{p}_i$ represent the center of the coordinate space and the momentum space of the ith nucleon, and L represents the corresponding wave packet width. The N body wave function can be represented by the direct product of the coherent states:

$$\Phi(\boldsymbol{r},\boldsymbol{r}_1,\cdots,\boldsymbol{r}_N,\boldsymbol{p}_1,\cdots,\boldsymbol{p}_N,t)=\prod_i \phi_i(\boldsymbol{r},\boldsymbol{r}_i,\boldsymbol{p}_i,t). \quad (2)$$

Antisymmetry is not considered here. The values adopted for the initial parameters can give all the nuclei of the projectile and target the correct density distribution and momentum distribution. The evolution of the system is derived from the generalized variational principle [36]:

$$S=\int_{t_1}^{t_2} \boldsymbol{L}[\Phi,\Phi^*]\mathrm{d}t, \qquad (3)$$

where $\boldsymbol{L}$ is the Lagrange function:

$$\boldsymbol{L}=\langle\Phi|\mathrm{i}\hbar\frac{\mathrm{d}}{\mathrm{d}t}-H|\Phi\rangle. \qquad (4)$$

The derivation of time here includes the derivation of the parameters $\boldsymbol{r}_i$ and $\boldsymbol{p}_i$. By taking the variation on the ac-

tion S, the evolution of the parameters $\boldsymbol{r}_i$ and $\boldsymbol{p}_i$ over time can be described by the Euler-Lagrange equation:

$$\begin{aligned}\frac{\mathrm{d}}{\mathrm{d}t}\frac{\partial\boldsymbol{L}}{\partial\dot{\boldsymbol{p}}_i}-\frac{\partial\boldsymbol{L}}{\partial\boldsymbol{p}_i}=0 &\quad\rightarrow\quad \dot{\boldsymbol{r}}_i=\frac{\partial\langle H\rangle}{\partial\boldsymbol{p}_i},\\[4pt]\frac{\mathrm{d}}{\mathrm{d}t}\frac{\partial\boldsymbol{L}}{\partial\dot{\boldsymbol{r}}_i}-\frac{\partial\boldsymbol{L}}{\partial\boldsymbol{r}_i}=0 &\quad\rightarrow\quad \dot{\boldsymbol{p}}_i=\frac{\partial\langle H\rangle}{\partial\boldsymbol{r}_i}.\end{aligned} \qquad (5)$$

Based on a Wigner transform on the wave function, the N body phase space distribution function can be expressed as:

$$f(\boldsymbol{r},\boldsymbol{p},t)=\sum_{i=1}^{n}\frac{1}{(\pi\hbar)^3}\mathrm{e}^{-\frac{[\boldsymbol{r}-\boldsymbol{r}_i(t)]^2}{2L}}\mathrm{e}^{-\frac{[\boldsymbol{p}-\boldsymbol{p}_i(t)]^2\cdot 2L}{\hbar^2}}. \qquad (6)$$

The evolution of the nuclei in the mean field over time in the system can be described by the Hamiltonian equation of motion:

$$\dot{\boldsymbol{r}}_i=\nabla_{\boldsymbol{p}_i}H,\dot{\boldsymbol{p}}_i=-\nabla_{\boldsymbol{r}_i}H. \qquad (7)$$

The statistical model GEMINI [37] can describe the decay series thermonuclear systems well. All decay chains adopt the Monte-Carlo method until the resulting products cannot decay further. The decay width can be calculated from the light-particle evaporation formula of Hauser-Feshbach [38] and the symmetric splitting transition formula of Moretto.

3   Results and discussion

The production cross section of Fe in the ^{86}Kr+^{181}Ta reaction at 64 MeV/nucleon is depicted in Fig. 1. For comparison, the experimental data and EPAX calculations are also shown. The simulation results are in good agreement with the experimental data, but the EPAX calculations underestimate the experimental data. The cross sections of fragments are mainly affected by the potential parameters in the model and the selection of collision events.

As the reaction conditions of the stimulated system, the impact parameters have an important effect on the reaction mechanism. Figure 2 shows the charge distribution of the ^{86}Kr+^{181}Ta reaction at 160 MeV/nucleon under different impact parameters. Given the same minimum value of impact parameter, more intermediate and large mass fragments are produced in the reactions with larger range of impact parameter, while the production cross sections of light mass fragments depend weakly on the impact parameter. The large difference between the fragments with large Z are due to the isospin effects in projectile fragmentations. This has been well understood in theory [40–44]. The isospin difference between the core and skirt of the projectile nucleus influences the difference between the neutron and proton density distribution in these areas, and induces the difference of fragments in large impact parameter ranges. The impact parameter used in this work is $b=0-10fm$.
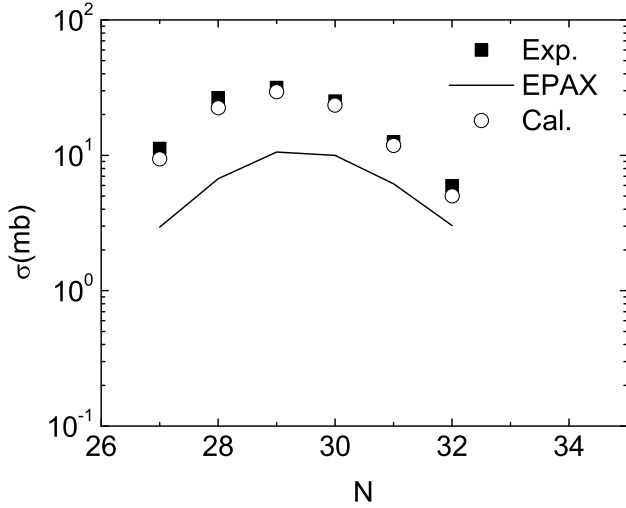
Fig. 1. The cross sections of the Fe isotopes predicted in this work (open circles), with the experimental measurements [39] (solid squares) and EPAX calculations (solid curves), in the ^{86}Kr+^{181}Ta reaction at 64 MeV/nucleon.
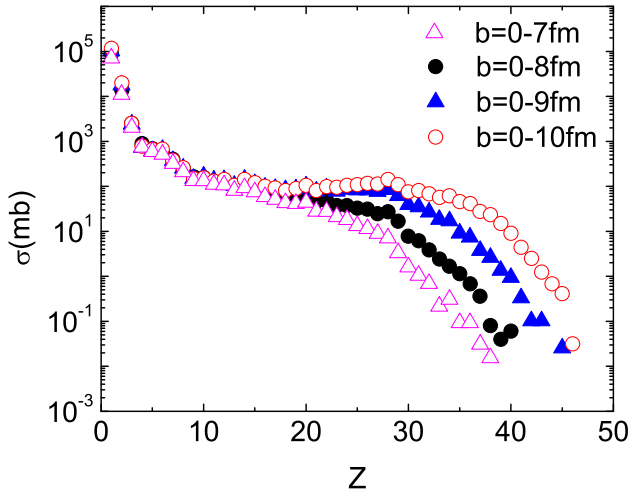
Fig. 2. (color online) The relationship between charge distribution and impact parameter in the ^{86}Kr+^{181}Ta reaction at 160 MeV/nucleon.

In order to investigate the energy and isospin dependence of the charge distributions, the isotopes of Si and P in each reaction system at different incident energies are calculated using the IQMD and GEMINI models. Figure 3 shows the cross section of the S isotopes produced by the ^{86}Kr+^{181}Ta reaction at incident energies of 80, 120 and 160 MeV/nucleon. Among them, ^{42}Si is a new nucleus that has not been synthesized experimentally. The results in the figure show that the peaks of the production cross sections of Si are located at $^{28-30}$Si at different incident energies. In the process of increasing the incident energy from 80 MeV/nucleon to 160 MeV/nucleon, the production cross section of $^{22-42}$Si decreases, and

the difference in the production cross section of ^{24}Si between the incident energies of 80 MeV/nucleon and 160 MeV/nucleon is obvious.
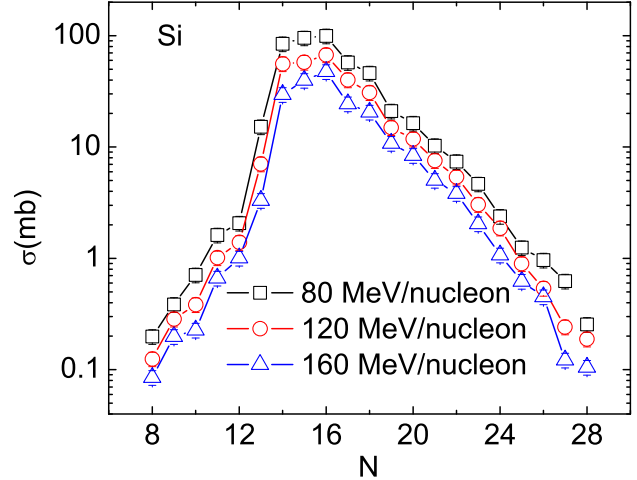
Fig. 3. (color online) The production cross sections of the Si isotopes for the ^{86}Kr+^{181}Ta reactions at 80 MeV/nucleon, 120 MeV/nucleon and 160 MeV/nucleon.

The production cross sections of the Si isotopes in the ^{86}Kr+^{181}Ta and ^{78}Kr+^{181}Ta reactions at 160 MeV/nucleon are plotted in Fig. 4. ^{41}Si is not produced in the ^{78}Kr+^{181}Ta reaction. The production cross sections of the isotopes near the proton drip line, such as $^{22-26}$Si in the ^{78}Kr+^{181}Ta reaction, are larger than those in ^{86}Kr+^{181}Ta, while the production cross sections of the isotopes near the neutron drip line, such as $^{35-40}$Si and ^{42}Si in the ^{86}Kr+^{181}Ta reaction, are larger than those in ^{78}Kr+^{181}Ta. The peak values at $^{28-30}$Si are roughly the same in both reactions.
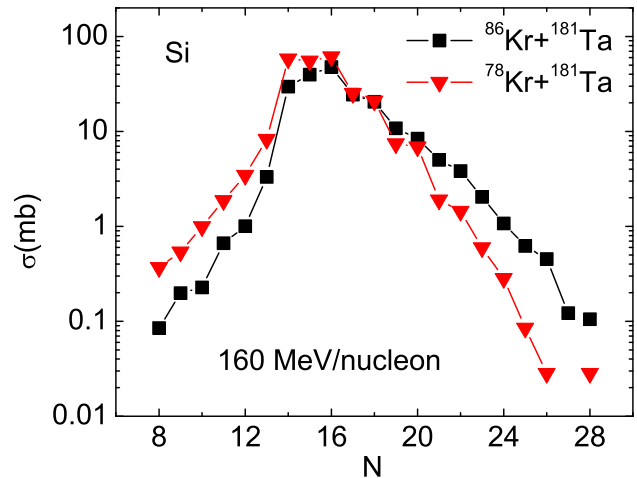
Fig. 4. (color online) The production cross sections of the Si isotopes in the ^{86}Kr+^{181}Ta and ^{78}Kr+^{181}Ta reactions at 160 MeV/nucleon.

Figure 5 shows the production cross sections of the P isotopes in the ^{86}Kr+^{181}Ta reactions at 80-160 MeV/nucleon. Among them, ^{46}P is an unknown nucleus that has not been synthesized experimentally. The results in the figure show that the peak positions of the production cross section of P are located at $^{31-33}$P at different incident energies. The production cross section of $^{24-46}$P decreases as the incident energy increases from 80 MeV/nucleon to 160 MeV/nucleon, while the gap in the production cross section of ^{27}P and ^{45}P between the incident energies of 80 MeV/nucleon and 160 MeV/nucleon is obvious.
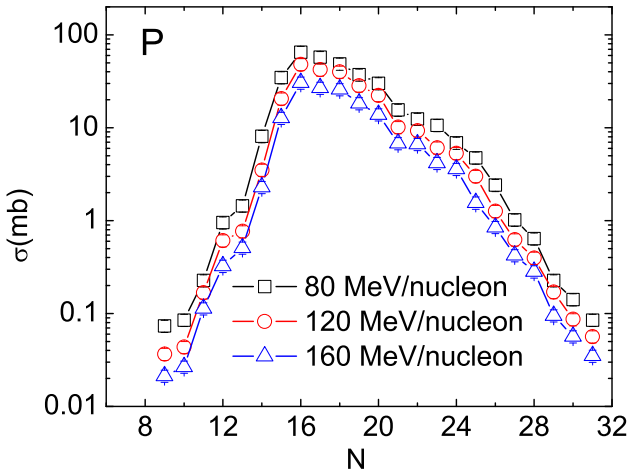
Fig. 5.   (color online) The production cross sections of the P isotopes for the ^{86}Kr+^{181}Ta reactions at 80 MeV/nucleon, 120 MeV/nucleon and 160 MeV/nucleon.
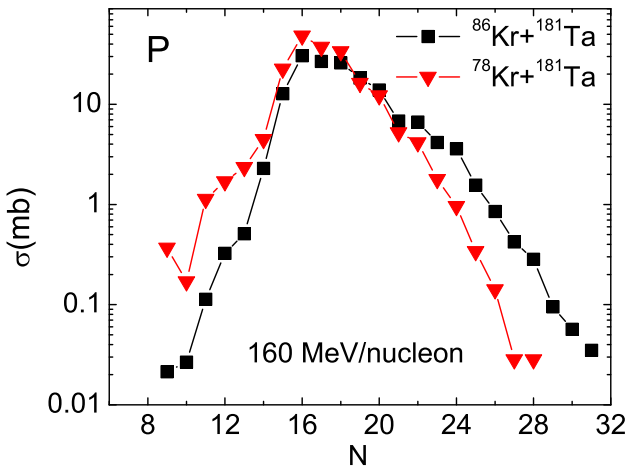
Fig. 6.   (color online) The production cross sections of the P isotopes in the ^{86}Kr+^{181}Ta and ^{78}Kr+^{181}Ta reactions at 160 MeV/nucleon.

The production cross sections of the P isotopes in the ^{86}Kr+^{181}Ta and ^{78}Kr+^{181}Ta reactions at 160 MeV/nucleon are depicted in Fig. 6. It can be noted that

the products of $^{44-46}$P are not found in the ^{78}Kr+^{181}Ta reaction, the production cross sections of the isotopes near the proton drip line, such as $^{24-28}$P, are larger than those in ^{86}Kr+^{181}Ta, while the isotopes near the neutron drip line, such as $^{38-43}$P, are produced more in the ^{86}Kr+^{181}Ta reaction. The peak values are located at $^{31-33}$P and are approximately the same in both reactions.

As can be seen from the above figures, more intermediate and large mass fragments are generated in the reactions with same minimum value but larger maximum value of impact parameter, while light mass fragments are less affected by the range of impact parameter. This is mainly due to the different reaction mechanisms of the system for different impact parameters. The system mainly undergoes fusion reactions when the impact parameters are small. As the impact parameters increase, the ratios of fast fission and deep inelastic collisions increase, resulting in more heavy fragments. The production cross sections of the isotopes of Si and P in the ^{86}Kr+^{181}Ta reaction generally decrease with increasing energy at 80 MeV/nucleon to 160 MeV/nucleon. For the same incident energy, the production cross sections of the isotopes near the proton drip line in the ^{78}Kr+^{181}Ta reaction are larger than those in the ^{86}Kr+^{181}Ta reactions, while the production cross sections of the isotopes near the neutron drip line in the ^{86}Kr+^{181}Ta reaction are larger than those in the other reactions. This phenomenon is mainly caused by the isospin effect in the nuclear multifragmentation, because the reaction conditions are exactly the same except for the neutron-proton ratio. For stable nuclides, the production cross sections in the two reactions are very close.

4   Conclusion

The fragment distribution in the reactions of ^{86}Kr+^{181}Ta and ^{78}Kr+^{181}Ta at 80-160 MeV/nucleon are studied via the IQMD model with the GEMINI model. It is found that intermediate and large mass fragments can be produced more in reactions with same minimum value but larger maximum value of impact parameter, while the impact parameter has less effect on the light mass fragments. This is mainly due to the different reaction mechanisms of the system for different impact parameters. The reaction proceeds via fusion when the impact parameters are small. As the impact parameters increase, the ratio of fast fission and deep inelastic collisions also increases. The production cross sections of the isotopes of Si and P produced in the ^{86}Kr+^{181}Ta reaction generally decrease with increasing energy. For the same incident energy, the production cross sections of the isotopes near the proton drip line in the ^{78}Kr+^{181}Ta reaction are larger than those in the ^{86}Kr+^{181}Ta reaction, while the production cross sections of the isotopes

near the neutron drip line in the neutron-rich system of ^{86}Kr+^{181}Ta are larger than those in the other systems. This phenomenon is mainly caused by the isospin effect of heavy ion reactions. For stable nuclides, the difference in the production cross section between the two reactions is very slight. These results may provide some guidance on how to select the reaction system and incident energy to produce an unknown nuclide and to conduct further relevant investigations.

References

1 P. Chomaz, F. Gulminelli, W. Trautmann, and S. J. Yennello, Eur. Phys. J. A, **30**: 275 (2006)
2 G. Chaudhuri, S. Mallik, and S. D. Gupta, Pramana: Journal of Physics, **82**: 907 (2014)
3 J. P. Bondorf, R. Donangelo, and I. N. Mishustin, Nucl. Phys. A, **443**: 321 (1985)
4 J. P. Bondorf, R. Donangelo, H. Schulz, and I. N. Mishustin, Nucl. Phys. A, **444**: 460 (1985)
5 D. H. E. Gross, Rep. Prog. Phys., **53**: 605 (1990)
6 S. Pal, S. K. Samaddar, and J. N. De, Nucl. Phys. A, **608**: 49 (1996)
7 D. J. Morrissey, B. M. Sherrill, Philos. Trans. R. Soc. A, **356**: 1985 (1998)
8 P. Danielewicz, R. Lacey, W. G. Lynch, Science, **298**: 1592 (2002)
9 K. A. Bugaev, M. I. Gorenstein, I. N. Mishustin, and W. Greiner, Phys. Lett. B, **498**: 144 (2001)
10 H. Jaqaman, A. Z. Mekjian, and L. Zamick, Phys. Rev. C, **27**: 2782 (1993)
11 J. N. De, X. Viñas, S. K. Patra, and M. Centelles, Phys. Rev. C, **64**: 057306 (2001)
12 J. Erler, N. Birge, M. Kortelainen, W. Nazarewicz, E. Olsen, A. M. Perhac, and M. Stoitsov, Nature, **486**: 509 (2012)
13 M. Thoennessen, Rep. Prog. Phys., **67**: 1187 (2004)
14 P. D. Cottle and K. W. Kemper, Phys., **5**: 49 (2012)
15 V. I. Goldanskii, Annu. Rev. Nucl. Part. Sci., **16**: 1 (1966)
16 J. Cerny and J. C. Hardy, Annu. Rev. Nucl. Part. Sci., **27**: 333 (1977)
17 R. Kalpakchieva et al, Eur. Phys. J. A, **7**: 451 (2000)
18 R. A. Kryger, A. Azhari, J. Brown et al, Phys. Rev. C, **56**: 1971 (1996)
19 M. Yu, H. L. Wei, Y. D. Song, and C. W. Ma, Chin. Phys. C, **41**: (2017) 094001
20 C. W. Ma and J. L. Xu, J. Phys. G: Nucl. Part. Phys., **44**: 125101 (2017)
21 B. Mei, Phys. Rev. C, **95**: 034608 (2017)
22 A. Ono and J. Randrup, Eur. Phys. J. A, **15**: 105 (2008)
23 G. Gulminelli and D. Durandet, Nucl. Phys. A, **615**: 117 (1997)
24 A. Z. Mekjian, Phys. Rev. C, **17**: 1051 (1978)
25 G. Fái G and J. Randrup, Nucl. Phys. A, **404**: 551 (1983)
26 S. E. Koonin and J. Randrup, Nucl. Phys. A, **474**: 173 (1987)
27 G. Peilert, H. Stöcker, W. Greiner, A. Rosenhauer, A. Bohnet, and J. Aichelin, Phys. Rev. C, **39**: 1402 (1989)
28 J. Aichelin, Phys. Rep., **202**: 233 (1991)
29 A. Ono, H. Horiuchi, T. Maruyama, and A. Ohnishi, Phys. Rev. C, **47**: 2652 (1993)
30 S. Ayik and C. Gregoir, Phys. Lett. B, **212**: 269 (1988)
31 J. Randrup and B. Remaud, Nucl. Phys. A, **514**: 339 (1990)
32 A. Ono, H. Horiuchi, T. Maruyama, and A. Ohnishi, Phys. Rev. Lett., **68**: 2898 (1992)
33 H. Feldmeier, Nucl. Phys. A, **515**: 147 (1990)
34 F. S. Zhang and E. Suraud, Phys. Rev. C, **51**: 3201 (1995)
35 L. W. Chen, F. S. Zhang, and G. M. Jin, Phys. Rev. C, **58**: 2283 (1998)
36 C. Hartnack, R. K. Puri, J. Aichelin et al, Eur. Phys. J. A, **1**:151 (1998)
37 R. J. Charity, M. A. McMahan, G. J. Wozniak, R. J. McDonald, and L. G. Moretto, Nucl. Phys. A, **483**: 371 (1988)
38 W. Hauser, H. Feshbach, Phys Rev., **87**: 366 (1952)
39 M. Mocko, M. B. Tsang, Z. Y. Sun et al, Phys. Rev. C, **76**: 014609 (2007)
40 C. W. Ma, H. L. Wei, J. Y. Wang et al, Phys. Rev. C, **79**: 014606 (2009)
41 C. W. Ma, H. L. Wei, S. S. han Wang et al, Phys. Lett. B, **742**: 19 (2015)
42 C. W. Ma, Y. D. Song, C. Y. Qiao et al, J. Phys. G: Nucl. Part. Phys., **43**: 045102 (2016)
43 C. W. Ma, H. L. Wei, and Y. G. Ma, Phys. Rev. C, **88**: 044612 (2013)
44 C. W. Ma, S. S. Wang, H. L. Wei, and Y. G. Ma, Chin. Phys. Lett., **30**: 052501 (2013)